An Investigation of Strut-Wall Intersection Losses

T. J. Barber*
Pratt & Whitney Aircraft, East Hartford, Conn.

A study of the intersection losses associated with the junction of a symmetric airfoil and a planar wall is reported. An experimental program, conducted in a low-speed air tunnel, provided detailed wake total pressure profiles as well as surface flow visualization photographs which define the overall flowfield. The behavior of the intersection losses was examined for dependence on flow incidence angle and strut contour. It was found that the endwall intersection losses were strongly dependent on the thickness of the incident boundary layers – thick boundary layers producing markedly lower losses than very thin incident boundary layers. A heuristic model of the flowfield, which explains marked differences between the thick and thin boundary-layer results, is also presented.

Nomenclature

b = strut chord
i = flow incidence angle
P_T = total pressure
q = dynamic head of upstream flow
R = local streamline radius of curvature
S = strut span
s = unit vector in streamwise direction
t = strut maximum thickness
δ = boundary-layer thickness
τ = strut gap, length of traverse
ρ = density
ν = kinematic viscosity
ξ = vorticity

Subscripts

s = streamwise component
n = normal component

I. Introduction

A PROBLEM that has been virtually neglected since the 1940's has been the loss generated by a strut intersecting a planar surface. This problem has been examined in terms of the viscous phenomenon in an intersection corner, but because of the low losses involved in airframe design, quantitative loss studies have not been conducted. However, when annular structures are mounted in gas turbine flow ducts, supported by struts crossing the flowpath, the multiplicity of strut wall intersections makes this loss nontrivial and renews interest in quantifying this effect.

At the present time, practically no published data exist on intersection losses. The primary quantitative source is Hoerner's[1] curves obtained from a 1942 NACA water tank towing experiment.[2] In this experiment, the intersection drag coefficients were found to be strongly dependent on flow incidence angle to the strut and were larger than the basic sectional drag coefficient of the struts tested. Hoerner furthermore indicated that the loss depended on the incident boundary-layer thickness.

Other investigations have concentrated on a description of the mechanism of the intersection in the neighborhood of the stagnation point. Johnston's[3] analysis defined the nature of the three-dimensional stagnation point and the formation of a horseshoe vortex produced by a cylinder/plane intersection. Schwind's[4] low Reynolds number flow visualization studies confirmed the presence of a single horseshoe vortex ahead of the stagnation point. As the Reynolds number was lowered, the vortex structure was more finely resolved into a number of essentially parallel vortices ahead of the intersection. Velocity surveys for a cylinder/flat plate intersection[5] and for a constant thickness strut with a semielliptic nose intersecting a flat plate[6] have been presented for flowfields at high-turbulent Reynolds numbers. Their traverse and flow visualization results again demonstrated the dominating effect of the horseshoe vortex. In another experimental study, Ram[7] examined the flow development of about a 15% thick NACA airfoil intersecting a flat plate. Isobar contours illustrated the development of the flow from the leading to trailing edge under the influence of a horseshoe vortex. These studies of the flow in the intersection region do not, however, provide a complete description of the flowfield, including the downstream character of the flow and, more importantly, do not give a quantitative description of the induced loss penalty.

This paper will present the experimental results obtained from a series of air tunnel experiments which examined the interaction of a strut with an endplate surface. Intersection loss mechanisms were evaluated by examining downstream total pressure surveys and flow visualization photographs. Quantitative loss results, as a function of intersection configuration and flow incidence angle, will be presented. The results will demonstrate the importance of the onset plate boundary layer on the strength of the horseshoe vortex and the effect of the interaction of the vortex with the pressure gradient induced by the strut thickness on the net loss.

II. Experimental Program

A low-speed air tunnel was used at atmospheric inlet conditions to examine the intersection losses of a number of 65 series symmetric struts, each having a 5 in. (12.7 cm) chord and a 6 in. (15.24 cm) span. Strut thickness-to-chord ratios, t/b, of 20% and 30% were used to determine any loss dependence on thickness. An inlet Mach number of 0.25 was generated from ambient conditions by a forced air compressor. A combination screen/honeycomb inlet system was used to limit the freestream turbulence level to less than 1%. Test section dimensions were 1 ft (30.48 cm) wide by 2 ft (60.96 cm) high. These dimensions insured an undisturbed flow over the strut, with almost no tunnel wall interaction. The primary intersection configuration studied is schematically shown on Fig. 1. A 3 ft long (91.44 cm) splitter plate was designed to produce a turbulent boundary-layer thickness δ/b of 0.12 at the strut leading edge. A survey of this boundary layer confirmed that a fully developed turbulent profile, corresponding to a test Reynolds number (Re_x) of

Presented as Paper 78-205 at the AIAA 16th Aerospace Sciences Meeting, Huntsville, Ala., Jan. 16-18, 1978; submitted Feb. 2, 1978; revision received May 1, 1978.

Index categories: Airbreathing Propulsion; Viscous Nonboundary-Layer Flows.

*Research Engineer, Turbine Research and Technology Group.

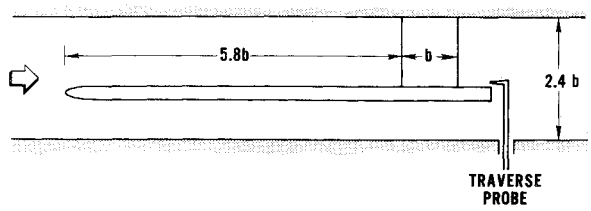

Fig. 1 Experimental configuration for strut intersection loss measurements, long leading edge plate, $M\infty = 0.25$.

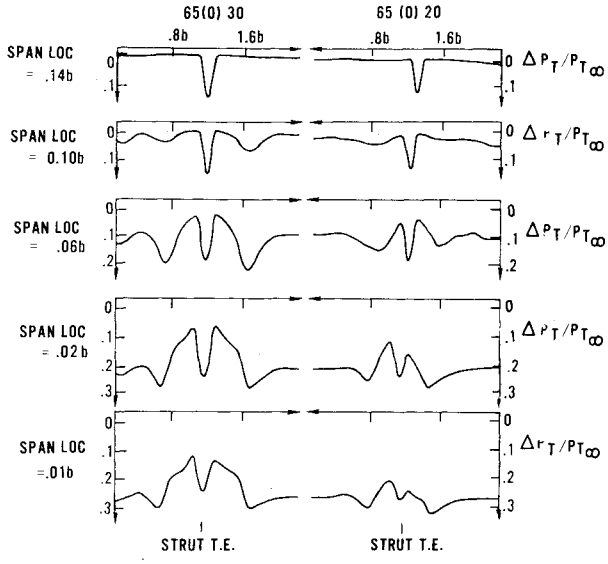

Fig. 2 Total pressure traverses measured $0.4b$ downstream from strut, $i = 0$ deg, $\delta = 0.12b$.

4×10^6, was produced. Total pressure traverses were taken across the strut wake 0.4 of a chord downstream from the strut trailing edge at many spanwise locations. The probe used was an externally chamfered boundary-layer probe and traversed within one-tenth of a strut chord from the endplate wall.

Typical traverse profiles for both struts, at zero incidence to the upstream flow, are shown in Fig. 2. The wake profiles are measured at discrete spanwise locations referenced dimensionally normal to the intersection surface. By $0.14b$ the total pressure profile has been reduced to the undisturbed two-dimensional strut wake profile. The displaced ordinate scale at $0.14b$ indicates the relative uniformity of the freestream flow. Although the strut in both configurations is at zero incidence to the upstream flow, the traverses indicate that a slight flow asymmetry was present. The strut wake is easily identified at the middle of each ΔP_T survey. The flow distortion on either side will be identified with the horseshoe vortex produced near the leading edge stagnation point of the strut and which has been convected downstream on either side of the strut and the secondary vorticity induced by the curvature of the incident shearing flow about the strut. The existence of the horseshoe vortex will be confirmed in the flow visualization results to be presented. The presence of the distributed secondary vorticity results in a massive redistribution of the flow, with local total pressure levels exceeding the levels found in the undisturbed plate boundary layer at that height, as seen by the levels at the ends of each traverse. The interaction of the horseshoe vortex and the secondary vorticity will be described in a later section. It is apparent that, without a careful survey, a false negative intersection loss could be measured. A quantitative integration, shown on Fig. 3, will demonstrate that the vortex itself does not introduce any appreciable loss, and that there is only a small intersection loss.

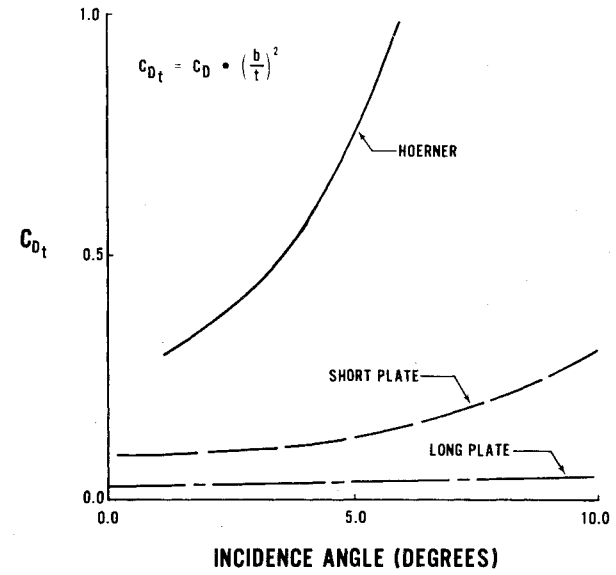

Fig. 3 Plot of intersection loss drag coefficients vs. flow incidence angle.

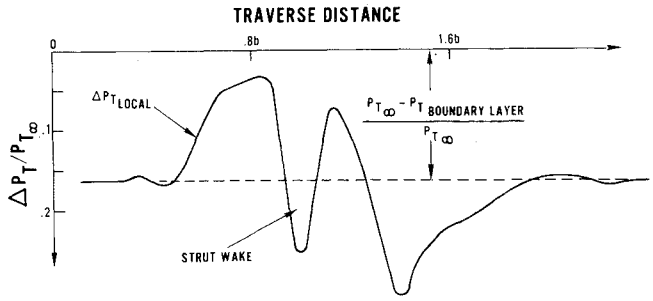

Fig. 4 Effect of flow incidence on downstream traverse, 65(0)30, $i = 10$ deg, $\delta = 0.12b$, span loc $= 0.04b$.

The drag of the intersection is obtained from a momentum balance of the forces on the model:

$$C_D = \frac{1}{q \cdot b \cdot S} \left[\int P_{T_{\text{bound. layer}}} d\tau dS - \int P_{T_{\text{local}}} d\tau dS \right] \quad (1)$$

The drag integral is a small quantity obtained from the difference of two large integrals. Testing was conducted for each strut over an incidence range of 0-10 deg. Intersection drag results for the 60(0)30 strut are shown on Fig. 3 and labelled "long plate." Little loss dependence on the incidence angle was found. The primary effect of thickness appears to be an increase in the vorticity-induced distortion, as illustrated in Fig. 2, while the effect of incidence is simply a distortion asymmetry, as shown by contrasting Fig. 2 with Fig. 4. In order to insure that the low-loss reading could not be attributed to neglecting the residual loss tied into downstream mixing of the swirling flow, an air angle and miniature kiel probe survey was made. Air angle results indicated that the swirl angle was limited to 8-10 deg. This was confirmed by the kiel probe results which indicated no measurable differences in total pressure from earlier traverse results.† The loss levels, however, are in order of magnitude lower than those found in the Hoerner data[1] for a 25% thick uncambered strut section (also shown on Fig. 3). Examination of the original source of Hoerner's data[2] indicated that a water tank drag balance study was conducted by NACA for the configuration shown

†Kiel probe has an accurate air angle tolerance up to 45 deg of swirl.

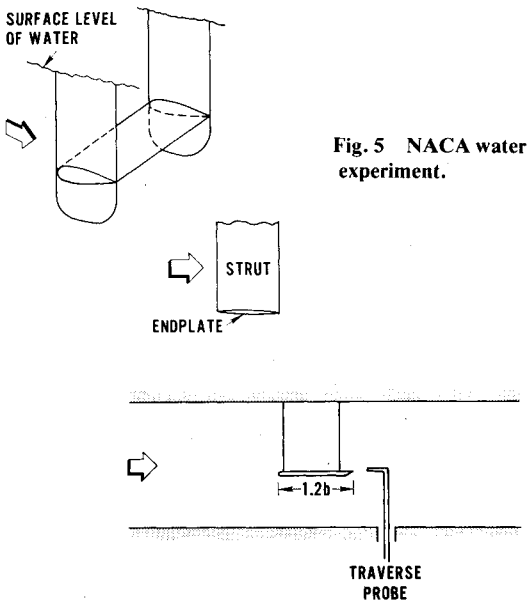

Fig. 5 NACA water tank towing experiment.

Fig. 6 Experimental configuration for strut intersection loss measurements, short leading edge plate, $M_\infty = 0.25$.

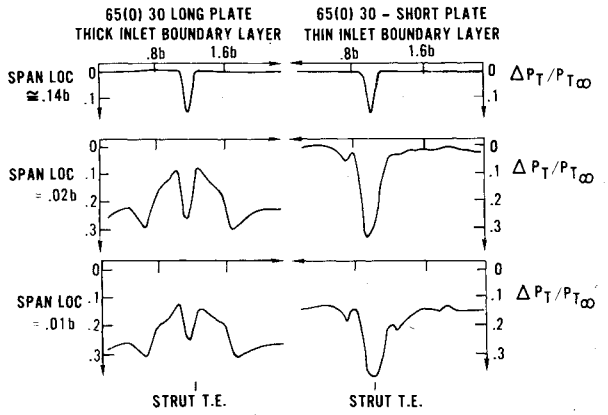

Fig. 7 Total pressure traverses measured 0.4b downstream from strut, $i = 10$ deg, $\delta = 0.12b$. Comparison of short and long.

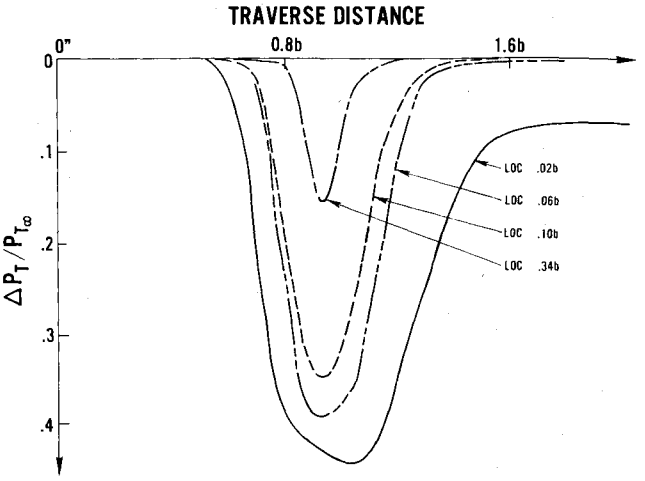

Fig. 8 Effect of flow incidence on downstream traverses, 65(0)30, $i = 10$ deg, $\delta = 0.12b$, $Z = 0$.

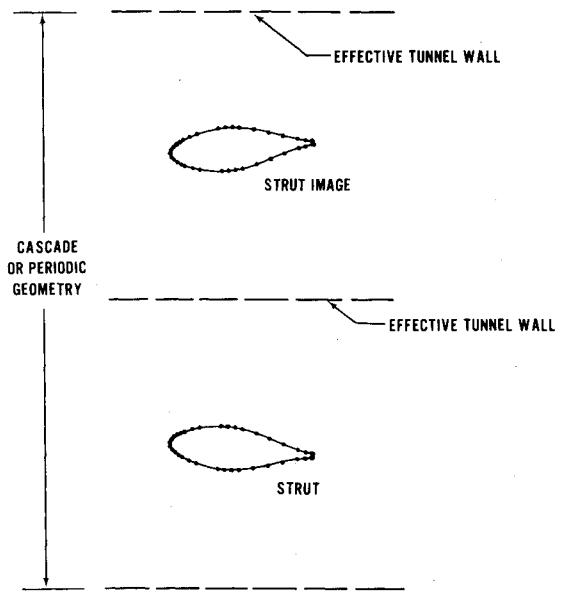

Fig. 9 Periodic representation of two struts producing virtual tunnel wall effect.

on Fig. 5. The most noticeable difference between this configuration and the generalized configuration shown on Fig. 1 appears to be the coincidence of the strut and endplate leading edges. Hoerner, however, presents these data as a generalized loss independent of configuration.

As a result of this discrepancy, an alternate intersection configuration, shown on Fig. 6, was traversed to examine the effect of a thin incident boundary layer on the intersection loss. A comparison of the total pressure surveys for the 65(0)30 strut, both in the long plate (thick boundary layer) configuration and short plate (thin boundary layer) configuration, is given on Fig. 7. In contrast to the earlier long plate results, this new configuration produced only a minimal growth in flow distortion lateral to the strut trailing edge. The basic two-dimensional viscous wake, however, has now grown significantly. The lack of distortion and the increased viscous wake are again clearly seen on Fig. 8. The traverse results for the 65(0)30 strut at 10 deg incidence show a dramatic buildup of the intersection loss, in marked contrast to the results shown on Fig. 4. The asymmetry of the 0.02b traverse may be an indication of a scale horseshoe vortex. Integration of the total pressure decrement for flow incidence angles of 0, 5, and 10 deg results in the increased drag results shown on Fig. 3 and labelled "short plate." The loss rise is almost entirely associated with the large strut wake growth. This will be demonstrated to be due to a large stall cell seen in the flow visualization photographs discussed later. The increased interference loss is of the order of the basic sectional drag of the strut, but not in the range of the results quoted by Hoerner. A possible reason for the higher loss levels reported by Hoerner is that this endplate had curvature, thus increasing the adverse pressure gradient over the rear part of the intersection, possibly causing a more severe stall cell to develop.

III. Flow Visualization

In order to explain the result obtained by traversing behind the intersection configurations, a series of lampblack and oil flow visualization studies were performed. Mylar drawing sheets were wrapped around and attached to the strut and splitter plate surfaces. A lampblack and oil suspension was painted onto the leading edges. This suspension flows back along the surface during testing. This technique[8] permits the sheets to be removed from the test section and viewed in a planar fashion. Irregularities in the oil flow patterns are usually due to extraneous effects; i.e., gravity, droplet size, tunnel start-up, and local Mylar lift-off from model surfaces. The lampblack traces can be considered only as approximations to the true streamlines. The results will be interpreted in a similar manner to the works of Schwind[4] and Johnston.[3]

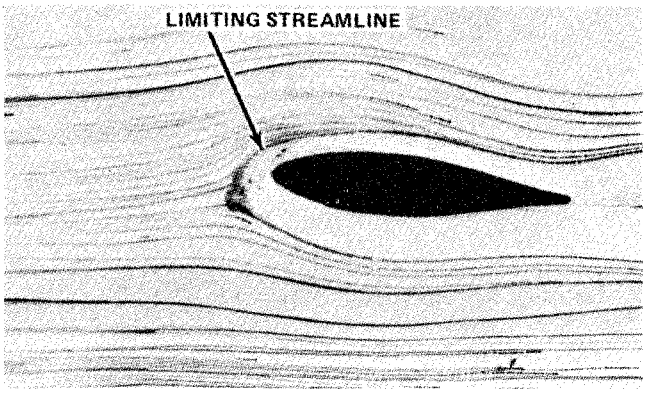

Fig. 10a Flow visualization of endplate surface, 65(0)20, $i = 10$ deg, $Z = 1.7b$.

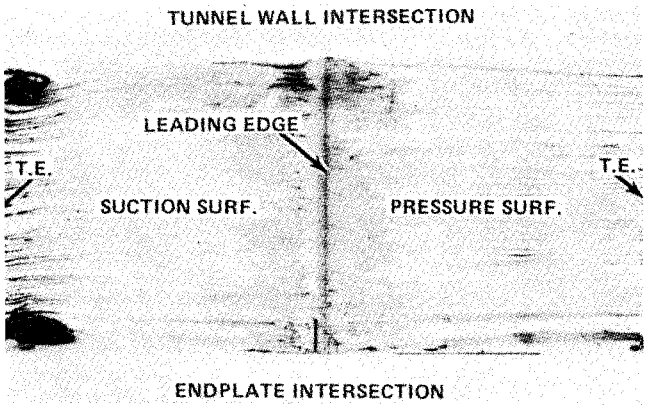

Fig. 10b Flow visualization of strut surface, 65(0)20, $i = 10$ deg, $Z = 1.7b$.

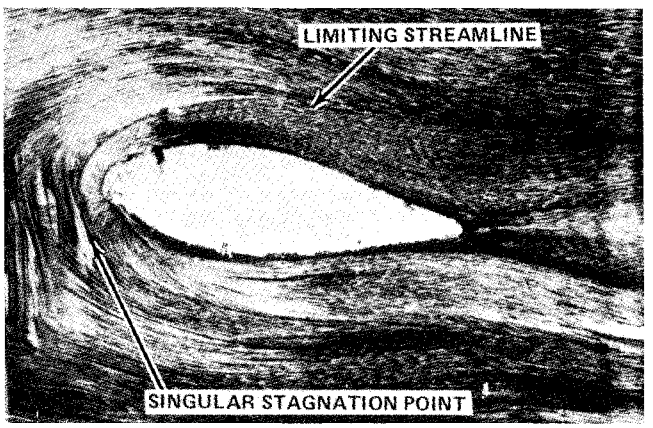

Fig. 11 Flow visualization of endplate surface, 65(0)30, $i = 10$ deg, $Z = 5.86b$.

The bulk of the flow visualization studies were conducted in an alternate air tunnel. The strut examined in this program was primarily the 65(0)20 section. The tunnel cross section was chosen smaller than that of the previously discussed tests to permit future studies into Mach number effects. Therefore, some tunnel/strut interaction was present. In contrast to the Allen-Vincenti[9] method for correcting measured drag levels to ideal two-dimensional conditions, a Douglas-Neumann[10,11] singularity superposition analysis was used to obtain correction conditions. Tunnel wall effects are simulated by calculating the flow over two airfoils at opposite angles of incidence in a cascade (Fig. 9). Incidence angles of 5 deg in this facility correct to approximately 10 deg in a noninterfering facility. All results to be presented are shown for the ideal 10-deg incidence condition.

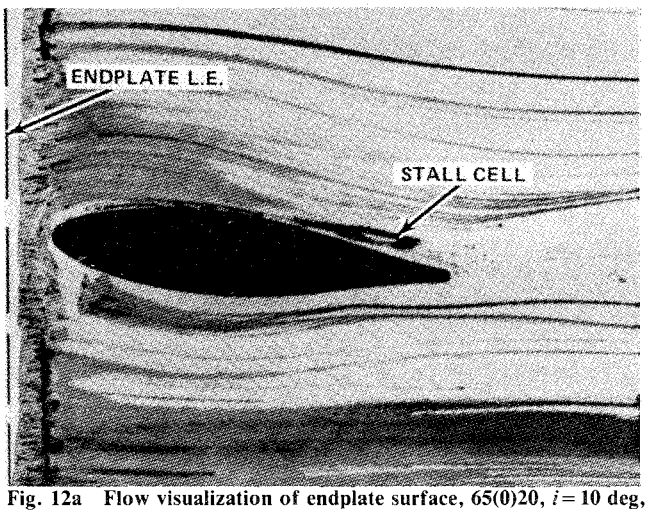

Fig. 12a Flow visualization of endplate surface, 65(0)20, $i = 10$ deg, $Z = 0$.

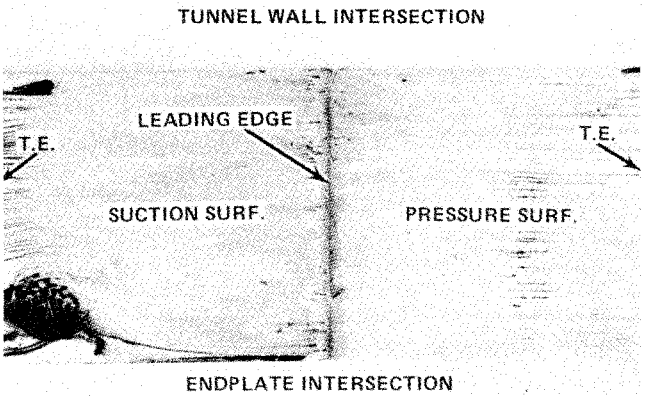

Fig. 12b Flow visualization of strut surface, 65(0)20, $i = 10$ deg, $Z = 0$.

A new degree of freedom offered by this facility was an ability to vary the distance between the endplate leading edge and the strut leading edge, Z. In the previous traverse study, Z was either 0 or $5.8b$; in this facility, Z is approximately $4.4b$ at the tunnel wall intersection with the strut and is varied from 0 to $1.7b$ at the plate intersection. Figure 10a illustrates the flow patterns on the splitter surface in the intersection region where $Z = 1.7b$ and $i = 10$ deg. Figure 10b illustrates the flow pattern on the strut for the same conditions. The effect of the long leading edge with its "thick" boundary layer is evident in the strut endwall pattern (Fig. 10a). On the plate surface, the effect of a horseshoe vortex standing off from the strut leading edge prevents the flow from the lower layers of the incident boundary layer from reaching the strut surface. Note that in Fig. 10b only localized small stall regions are present on the suction surface of both the splitter intersections ($Z = 1.7b$) and the tunnel wall intersection ($Z = 4.4b$). The details of the generation of the vortex were made more visible in Fig. 11, taken in the traversing air-tunnel facility. Here a 65(0)30 strut was set at 10 deg incidence to accentuate the offset of the leading edge stagnation point.

In contrast to the long plate-type intersections, Figs. 12a and 12b illustrate the flowfield in which the strut and splitter plate have nearly coincident leading edges ($Z = 0$, $i = 10$ deg). The suction surface intersection patterns (Fig. 10b) are markedly different, with a large stall cell on the strut/splitter plate endwall, indicating a significant increase in the interference loss. This corroborates the integrated traverse data. A laminar separation bubble along the leading edge of the splitter is found upstream of the strut leading edge field in regions laterally removed from the strut leading edge. The pressure field of the strut has altered this transition in the

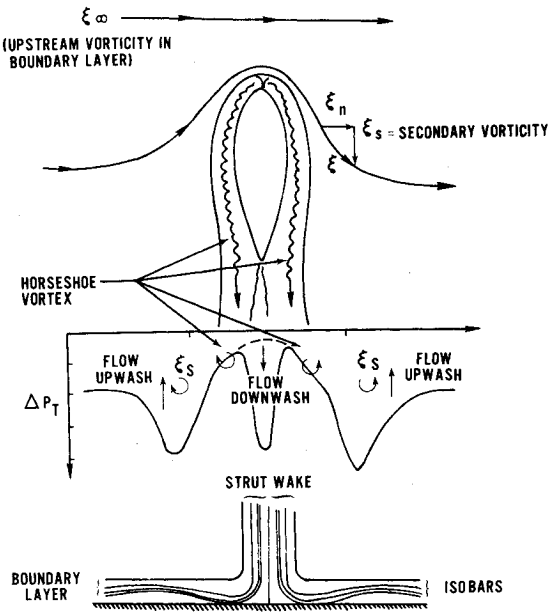

Fig. 13 Schematic overlay of intersection induced flowfield, 65(0)30, $i = 0$ deg, $Z = 5.86b$.

region near the leading edge. The plate wall, moreover, does not show any appreciable horseshoe vortex. In this case, the wall flow appears to be flowing onto the strut suction surface.

IV. Model of Strut Intersections

The intersection of a boundary-layer flow over a flat wall, through which a symmetric strut projects at a right angle, results in a complex three-dimensional flowfield. The downstream flowfield indicates that the flow has undergone a loss in total pressure as well as a distortion of the upstream Bernoulli surfaces. The incident boundary layer can be viewed as a distribution of line vorticity filaments, ξ_∞, shown on Fig. 13. As the flow nears the strut, the line element is deflected and stretched about the leading edge in the manner schematically shown in the figure. The inviscid path of the vortex element has been calculated (for a variety of strut shapes) using a linearized secondary vorticity model.[12] The induced or streamwise component of vorticity, ξ_s, arises from the deflection of the upstream flow by the strut contour. It can be analytically determined that the vortex element path is a monotonic function decreasing from the strut leading edge. In the more realistic situation, however, the flow is not inviscid. The more general streamwise vorticity description has been analyzed by Louis,[13] Lakshminarayana and Horlock,[14] resulting in the following relation

$$\frac{\partial}{\partial s}\left(\frac{\xi_s}{q}\right) = -\frac{2\xi_n}{qR} + \nu\frac{s\cdot\nabla^2\xi}{q} \qquad (2)$$

Louis demonstrated that such a flow can be considered as s superposition of the inviscid or potential term and a viscous vorticity dissipation term.

The dominance of each vorticity term is evident in Fig. 13, where a flow visualization schematic of Fig. 11 is overlapped with a typical traverse from Fig. 2. The inner or horseshoe vortex is of large scale (in terms of the boundary-layer thickness), but is of weak strength. The distributed secondary vorticity, however, dominates the flow, resulting in a downwash contribution at the midtraverse location and an upwash component at either end of the traverse. This explains the flow distortions shown in Fig. 2. The isobar plots, shown at the bottom of Fig. 13, are similar to those found in Ram.[7] The lateral distortion effect of the secondary vorticity is appreciably masked and, therefore, not discussed by Ram.

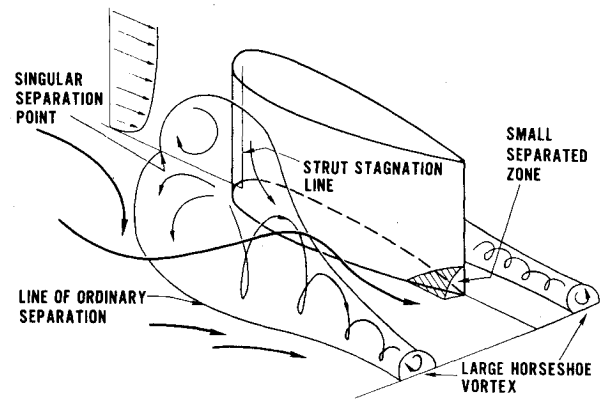

Fig. 14 Proposed model of thick boundary-layer-strut interaction.

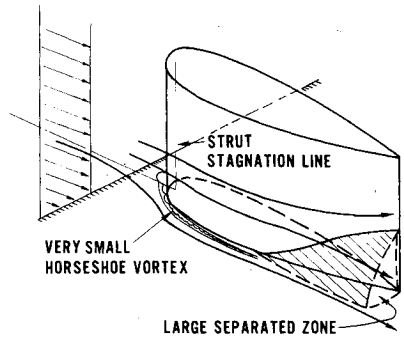

Fig. 15 Proposed model of thin boundary-layer-strut interaction.

The viscosity-dominated horseshoe vortex results in a point of separation which will exist on the wall upstream of the strut leading edge because the low momentum flow in the boundary layer is unable to sustain its forward motion against the pressure rise produced by the strut leading edge. This singular separation point is analogous to a two-dimensional separation point in that the wall shear stress (τ_w) goes to zero and flow reversal appears downstream. This reversal, combined with the incoming boundary layer, forms a swirling flow near the leading edge, with the fluid near the endwall flowing away from the strut (outward) and the fluid further from the endwall flowing toward the strut (inward).

The continual flow of upstream fluid fills the leading edge separation zone and convects the older swirling downstream on either side of the strut fluid (see Fig. 14). The combination (near the wall surface) of the outward swirling flow with the wall boundary-layer flow forms a line of "ordinary separation." This line is the locus of convergence of the limiting streamlines from which the flow will leave the surface of the endwall. Ordinary separation differs significantly from singular or two-dimensional separation in that τ_w does not approach zero and no flow reversal is observed immediately downstream. The swirling flow convected downstream is called a horseshoe vortex.

The path of the horseshoe votex is determined by the interaction of the onset boundary-layer flow with the strut pressure field, while the strength is dependent on the edge velocity and the local boundary-layer thickness. The size of the vortex will determine the nature of the downstream flowfield as well as the intersection loss penalty. The experimental wake traces, obtained in the low-speed air tunnel, indicated that the horseshoe vortex contribution is dominant in flows where the onset boundary layer is of the order of the strut maximum thickness. A significantly different result is observed for thin boundary flows, where data indicate that the viscous wake due to corner separation is dominant (Fig. 15).

The data suggest that the low-loss condition is obtained only in intersections with flows having freestream vorticity. It appears that a large weak vortex is generated by a thick boundary layer and, as it moves away from the intersection corner, acts as a barrier preventing low-momentum boundary-layer flow from filling the corner. This fluid leaves the surface at the limit line and is convected downstream rather than stagnating in the intersection corner. High-momentum flow, on the other hand, passes over the vortex cells and fills the corner region. This fluid is capable of sustaining high adverse pressure gradients present toward the rear of the strut before separating. In the case of a small-scale vortex, which would be produced by a thin onset boundary layer, no freestream vorticity is present and it appears that the low-momentum flow is now unrestrained by a vortex and fills the intersection corner. This fluid is less capable of sustaining the high adverse pressure gradient on the aft section of the strut and leads to early separation and high loss. The model just described also explains the relative differences in downstream distortion patterns observed for thick and thin onset boundary-layer intersection flows.

The vorticity of the vortex is known to be inversely proportional to the layer boundary-layer thickness (U/δ). In the small-scale vortex configuration, it is possible that the large swirl component will induce separation of the corner boundary layer. Determination of the specific mechanism involved in the separation process would require high-response instrumentation, which is beyond the scope of this planned study. A similar endwall process has been observed in turbine cascades,[8] where the horseshoe vortex and the turning-induced secondary vorticity are rolled up by the cross-channel pressure gradient. In this case, it was also impossible to determine whether the horseshoe vortex or the endwall boundary layer was primary agent in producing the turbine endwall loss.

V. Summary and Conclusions

The results of the experimental traverse and flow visualization studies of the strut and endplate intersection have demonstrated that the resultant losses are significantly different and the flow behavior is more complicated than indicated by previously documented studies. The intersection losses are found to be governed by the thickness of the incident boundary layer and the size of the resultant horseshoe vortex. A thin incident boundary layer results in:

1) a large intersection loss
2) a strong loss dependence on flow incidence angle
3) a very small horseshoe vortex.

A thick boundary layer, on the other hand, results in:

1) a small intersection loss
2) a weak loss dependence on flow incidence angle
3) a large horseshoe vortex.

In either case, however, it should be noted that a net loss increase is observed due to the intersection.

In addition to quantifying the losses produced by a strut intersection, the data have indicated that a flow distortion, extending laterally more than one strut chord, can be produced downstream of the intersection. This distortion extends into the flow only as far as the incident shear and can be modelled by inviscid secondary flow theory. In most situations, the shear is simply a boundary layer; therefore, the distortion will be confined to a small region of the total flow. However, when the shear is of the order of the flow area, a large-scale lateral distortion will be imposed on any downstream geometrics intersecting the flowpath.

References

[1] Hoerner, S.F., *Fluid Dynamic Drag,* Vol. 11, 1965, Chap. 8, pp. 10-11.

[2] Benson, J.M., Land, N.S., and Havens, R.F., "Tank Tests of Ship Propeller Strut Sections," NACA 4105/72, April 1942.

[3] Johnston, J.P., "The Turbulent Boundary Layer at a Plane of Symmetry in a Three-Dimensional Flow," *Journal of Basic Engineering,* Vol. 82, Sept. 1960, pp. 622-627.

[4] Schwind, R.G., "The Three-Dimensional Boundary Layer Near a Strut," MIT GTL Rept. No. 67, 1962.

[5] Ram, V.V., "Untersuchungen uber die Eckengrenzschicht an einem Kreiszylinder mit Seitenwand," Bericht 63/64, Institut fur Stromungsmechanik, Technische Hochschule Braunschweig, 1963.

[6] Shabaka, I., "A Preliminary Experimental Investigation of Turbulent Flow in a Simplified Wing-Body Junction," Imperial College Aero Rept. 75-05, 1975.

[7] Ram, V.V., "Experimentelle Untersuchungen der Stromung entlang einer rechtwinkligen Ecke Zwichen einen Profil und einer ebenen Seitenwand," Bericht 63/17, Institut fur Stromungsmechanik, Technische Hochschule Braunschweig, 1963.

[8] Langston, L.S., Nice, M.L., and Hooper, R.M., "Three Dimensional Flow Within a Turbine Cascade Passage," ASME Paper 76-GT-50, 1976.

[9] Allen, H.J. and Vincenti, W.G., "Wall Interference in a Two Dimensional Flow Wind Tunnel with Consideration of the Effect of Compressibility," Nat. Adv. Comm. Aero., Wash., Rept. 782, 1944.

[10] Smith, A.M.O. and Pierce, J., "Exact Solution of the Neumann Problem Calculation of Noncirculatory Plane and Axially Symmetric Flow About or Within Boundaries," Douglas Aircraft Co. Rept. ES26988, 1958.

[11] Geising, J.P., "Extension of the Douglas Neumann Program to Problems of Lifting Infinite Cascades," Douglas Aircraft Co. Rept. LB31653, 1964.

[12] Hawthorne, W.J., "The Secondary Flow About Struts and Airfoils," *Journal of the Aeronautical Sciences,* Vol. 21, Sept. 1954, p. 588.

[13] Louis, J.F., "Rotational Viscous Flow," *Proceedings of 9th International Congress of Applied Mechanics,* Vol. 3, 1956, p. 306.

[14] Lakshminarayana, B.L. and Horlock, J.H., "Generalized Expressions for Secondary Vorticity Using Intrinsic Coordinates," *Journal of Fluid Mechanics,* Vol. 59, 1973, p. 97.